JOURNAL OF SOLID STATE CHEMISTRY 72, 293–302 (1988)

Investigations of the Bulk Defect Chemistry of Polycrystalline Tin(IV) Oxide*

J. MAIER

Max-Planck-Institut für Festkörperforschung, D-7000 Stuttgart, Federal Republic of Germany

AND W. GÖPEL

Institut für Physikalische und Theoretische Chemie der Universität, D-7400 Tübingen, Federal Republic of Germany

Received March 24, 1987

The bulk defect chemistry of polycrystalline SnO_2 has been investigated systematically by impedance spectroscopy. Nominally pure and In- and Sb-doped materials were shown to be stable in the rutile structure over the entire temperature range (500–900°C). Lattice constants were determined as a function of temperature. Defect chemistry can be described consistently by assuming fully ionized oxygen vacancies and conduction electrons as native defects. In the O_2 partial pressure range between 0.02 and 1 bar, intrinsic behavior was observed with a characteristic exponent of $-\frac{1}{6}$ for $T > 800$°C in nominally pure oxides, whereas at lower temperatures acceptor impurities dominate the conductivity with a characteristic exponent of $-\frac{1}{4}$. In agreement with the defect model proposed, the extrinsic conductivity behavior changes toward intrinsic conductivity behavior with decreasing partial pressure at constant temperature. Heavy In doping (In'_{Sn}) increases the acceptor influence, i.e., lowers the (electronic *n*-) conductivity and extends the extrinsic regime. Weak Sb doping ($Sb^{\cdot}_{Sn}$) has a donor influence and causes an increase in the conductivity. Since in this case foreign acceptor defects still form the majority of carriers, the transition between extrinsic and intrinsic behavior occurs at lower temperatures but at the same conductivity value. The temperature dependence also reflects this transition and yields enthalpy values for oxygen incorporation of about 1.1 eV per electron.

1. Introduction

There is great interest in SnO_2 because of its advantageous transport properties, with particular emphasis on its properties as a sensor for reducing gases (*1*). Although there exists a large amount of literature concerning low-temperature gas sensing properties, systematic experiments on the basic defect chemistry are still lacking. Intrinsic bulk defects of SnO_2 do, however, influence all charge transfer reactions during gas sensing at low temperatures. In the present study of bulk defects we performed complex impedance measurements at different temperatures and O_2 partial pressures for pure and differently doped SnO_2.

Most authors agree that oxygen vacancies constitute the majority of native ionic defects in SnO_2 (*2–4*). The energy difference between the oxygen donor levels and the edge of the conduction band is probably

* Dedicated to Professor Albrecht Rabenau on the occasion of his 65th birthday.

0022-4596/88 $3.00

not larger than 0.1 eV (*2, 3–5*). SnO_2 is an *n*-type semiconductor even at oxygen pressures of 150 bar (*6*). This is consistent with the large bandgap. Values between 3 and 4 eV may be found in the literature (*5, 7, 8*). Most investigations, however, suggest a value of 3.5 eV (*8–10*). In a detailed study, Kohnke derived 3.54 eV with a temperature coefficient of -6×10^{-4} eV/K (*5*). These values represent the (free) enthalpy of formation of charge carriers, i.e., electrons e' and holes $h^{\cdot}$:

$$0 \rightleftharpoons e' + h^{\cdot} \qquad (1)$$

For many oxides, this reaction may, to a first approximation, be assumed to characterize the energy of electronic charge transfer from O^{2-} to the metal cation (here Sn^{4+}), i.e., from the valence $2p(O^{2-})$ to the conduction $5p(Sn^{4+})$ band. There is, however, some evidence in the literature (*9*) that the situation is more complex for SnO_2. The energy for oxygen incorporation, which is the dominant defect-inducing process in most SnO_2 materials, is not yet known, but is expected to be lower than the bandgap energy. The sensing mechanism at low temperatures is assumed to involve trapping of electrons by adsorbed oxygen (*1, 11, 12*). As a result, the concentration of free electronic charge carriers (e') is strongly reduced in the boundary regions. This space charge effect can be monitored easily by resistance measurements. Fortunately, bulk diffusion of defects is very low at room temperature and causes only a weak drift in the total resistance of the sample.

To optimize the sensor properties of SnO_2, it is important to understand the thermodynamic and kinetic behavior of the system at the phase boundary, in the boundary region, and in the bulk. We plan to investigate these subjects systematically by comparing temperature-dependent solid/gas interactions with single crystals, polycrystalline samples, and thin films and to present these results in a series of publications. This paper deals with the defect chemistry of bulk SnO_2 under equilibrium conditions.

Because of low diffusion coefficients at temperatures below 900°C, we choose polycrystalline samples as specimens. At temperatures above 1000°C, Schottky disorder and formation of SnO are assumed to play an important role (*13*). There also exists in the literature some confusion concerning crystal modifications of SnO_2. Even at normal pressures, the existence of different modifications has been postulated over the entire temperature range investigated in the present study (*8, 14*). In contrast to these findings, several other authors assume SnO_2 to be stable in the rutile structure ($SnO_{6/3}$) only and attribute experimentally observed changes in the lattice parameters to thermal expansion (*13*).

2. Experimental

2.1. Materials

Two kinds of nominally pure SnO_2 have been used, SnO_2 (Kelpin, 99.9%) and SnO_2 (Ventron, 99.998%). To obtain a fine powder, SnO_2 has been ground in a ball mill (agate). In-doped material has been obtained by dissolving In in HNO_3 (Merck, suprapure), mixing the solution with SnO_2 (Kelpin) powder, neutralizing with ammonia (Merck, suprapure), and evaporating the volatile compounds. Sb-doped material has been obtained by oxidizing Sb with HNO_3 to Sb_2O_5 (aq), suspending the latter in water, mixing the solution with SnO_2 (Ventron), and evaporating the water. The materials were pressed into pellets by cold isostatic pressing at $P = 10$ kbar and annealed at 900°C for 15 h in a quartz vessel together with excess SnO_2 powder, with the latter covered with an alumina crucible. As-prepared SnO_2 ceramic material obtained by this procedure was white, homogeneous, and of good mechanical stability and exhibited a grain size of 1–5 μm. Sintering

at higher temperatures led to SnO_2 with a density of 70% of the theoretical bulk value. The difficulty in obtaining denser SnO_2 ceramics is well known (*5*). Sintering at higher temperatures was avoided because of the possible onset of the (Schottky) reaction which creates additional Sn vacancies and, moreover, hinders the sintering effect (*15*). The pellets were polished with a diamond paste and contacted on both sides by vapor-deposited Pt or Ag.

2.2. *Methods of Investigation*

X-ray diffraction experiments were performed at different temperatures with the Guinier–Simon technique. Further sample characterization was possible by inductive coupled plasma emission spectroscopy (ICP), X-ray fluorescence (XRF), and scanning electron microscopy (SEM). Electrical conductivities were measured by impedance spectroscopy at frequency between 100 Hz and 10 kHz (Wayne Kerr 3905) and between 5 Hz and 13 MHz (HP 4192A) as a function of temperature and oxygen partial pressure. The latter was adjusted by O_2/Ar mixtures in the range $P = 10^{-3}$ to 1 bar and by CO/CO mixtures for establishing lower partial pressures. Impedance measurements have been evaluated by adjusting different system functions.

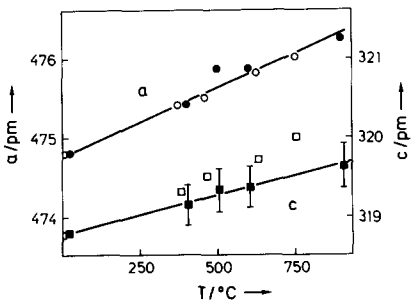

FIG. 1. Lattice constants of SnO_2 (rutile) as a function of temperature. The open symbols refer to Ref. (*13*).

TABLE I

RESULTS OF THE CHEMICAL ANALYSIS

Material	Additive	Analysis
SnO_2 (Kelpin)	—	0.4 m/o Fe[b] (0.6 m/o Al,[b] ground)
SnO_2 (Ventron)	—	0.3 m/o Fe,[b] 0.2 m/o Al[b]
SnO_2 (Sb_2O_5)	0.03 m/o Sb[a,b]	0.02 m/o Sb,[b,c] 0.35 m/o Fe,[b] 0.55 m/o Al[b]
SnO_2 (In_2O_3)	0.8 m/o In[a]	0.5 m/o In,[b] 0.27 m/o Fe,[b] 0.17 m/o Al[b]

Note. m/o denotes mole percent.
[a] Weight.
[b] ICP.
[c] XRF.
[d] SEM.

3. Results

The X-ray diffraction experiments did not give any hint of a phase transition of $SnO_{6/3}$ (rutile) as claimed earlier in the literature (*8*). We observed a continuous increase in the lattice constants as shown in Fig. 1. The *a* constant is in good agreement with the values reported in Ref. (*13*), whereas our *c* values are slightly smaller.

Table I shows results of the chemical analysis of the final products. The values for the dopants are consistent with the initial (educt) concentrations.

Table I also indicates the presence of a large amount of acceptor impurities introduced by the preparation. The analysis indicates that most In is localized in the grain boundaries since during the dissolution of $SnO_2(In_2O_3)$ the major portion of In is dissolved at the beginning. The same is assumed to hold for the other impurities. For the conductivity measurements reported here, Pt electrodes have been used since the Ag electrodes cause a strong reduction of SnO_2. The latter results from the formation of Ag/Sn alloys observed at the low O_2 partial pressures adjusted in CO/CO_2 mixtures. According to thermodynamic values and the vapor pressure of SnO, the low oxygen partial pressure alone cannot account for this reduction.

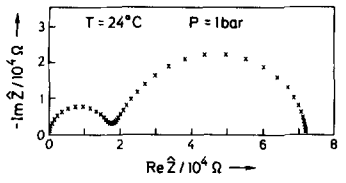

FIG. 2. Impedance spectrum of SnO_2 (5 Hz to 10 MHz) with real (Re $\hat{Z}$) and imaginary (Im $\hat{Z}$) parts of the impedance $\hat{Z}$. Frequency increases from right to left. The diameter of the high-frequency semicircle equals the bulk resistance.

Figure 2 shows an impedance plot for SnO_2 obtained at 24°C and $P(O_2)$ = 1 bar. Here, the available frequency range is used most favorably. The right semicircle can be attributed to boundary effects and is not discussed in detail. The left, high-frequency semicircle is attributed to the bulk impedance. Highly conducting boundary layers which would short-circuit the bulk and influence the high-frequency semicircle [as observed, e.g., for AgBr and AgCl (*16*)] are not observed here. The characteristic capacitance is basically constant under all experimental conditions (~15 pF). This excludes the influence from boundaries such as space charge layer effects. Unfortunately the stray capacitance of the apparatus does not allow evaluation of the bulk dielectric constant. The nonzero intercept to the left semicircle has been taken as the bulk resistance.

The partial pressure dependence of the bulk conductivity is illustrated by log σ-versus-log P plots in Figs. 3–6. The temperature dependence is illustrated by log σ-versus-$1/T$ plots in Fig. 7. The σ values characterize equilibrium conditions. Typical times to adjust these equilibria are discussed briefly in Section 4.5.

4. Discussion

The σ values in Figs. 3–6 are low compared with conductivity values of single crystals (*2, 3*). This is caused by the high porosity and may be described by blocking factors, as they were observed in two-phase conductor/insulator materials (*17*).

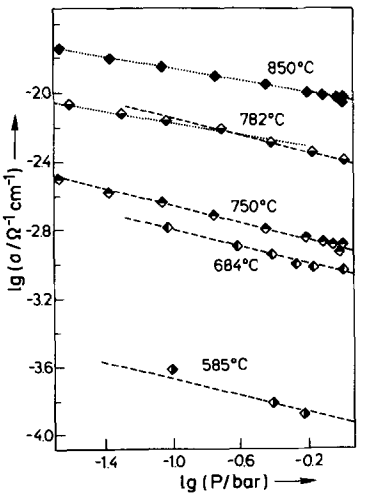

FIG. 3. Conductivity of SnO_2 (Kelpin) as a function of O_2 partial pressure for different temperatures. Dashed and dotted lines refer to extrinsic and intrinsic behavior, respectively.

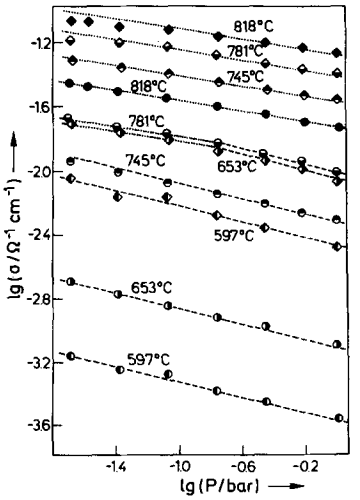

FIG. 4. Conductivity of SnO_2 (Ventron) (round symbols) and of SnO_2 (Sb_2O_5) (rhombic symbols) as a function of O_2 partial pressure for different temperatures. Dashed and dotted lines refer to extrinsic and intrinsic behavior, respectively.

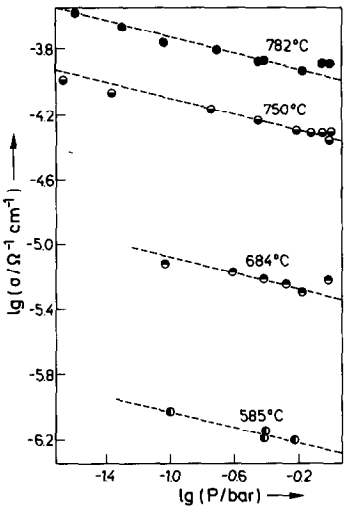

FIG. 5. Conductivity of SnO_2 (In_2O_3) as a function of O_2 partial pressure for different temperatures. Dashed and dotted lines refer to extrinsic and intrinsic behavior, respectively.

The blocking factors take into account the number of blocked nonpercolating pathways. Without more detailed microscopic information about the grain structure, this factor may be estimated only roughly. The absolute σ values are therefore not considered and an evaluation of entropy values and mass action constants is not given in this paper. In all following evaluations and particularly in the evaluation of the partial pressure dependence of σ, absolute values are not important.

4.1. *Defect Equilibria*

Because of the high valency and high coordination number of Sn^{4+} in the rutile structure, the formation of tin defects is only probable at high temperatures. The formation of tin vacancies (which are frozen-in at lower temperatures) and of oxygen vacancies in a Schottky-type reaction

$$Sn_{Sn} + 2O_O \rightleftharpoons SnO + \tfrac{1}{2}O_2 + V''''_{Sn} + 2V^{\cdot\cdot}_O \quad (2)$$

is assumed to be significant at temperatures

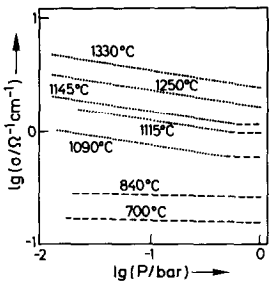

FIG. 6. Conductivity of SnO_2 made from $SnCl_4$ as a function of O_2 partial pressure for different temperatures according to Ref. (*2*). Dashed and dotted lines refer to extrinsic and intrinsic behavior, respectively.

above 1100 K, thereby causing an anomalous increase in the lattice constants (*13*). The dense rutile structure suggests the absence of interstitial oxygen defects. In agreement with other authors we assume oxygen vacancies as native ionic majority defects (*2*). Hall experiments (*3, 4*) indicate that SnO_2 is an *n*-type conductor even at high O_2 pressures and that—according to the large bandgap—hole concentrations can be neglected. Therefore, the interaction

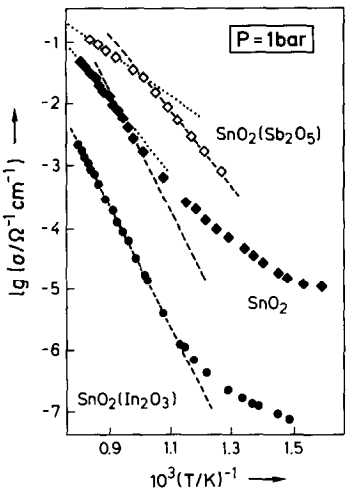

FIG. 7. Conductivity of different SnO_2 materials as a function of temperature, $P(O_2) = 1$ atm. The low-temperature range (300–600 K) is not shown. Dashed and dotted lines refer to extrinsic and intrinsic behavior, respectively.

of SnO_2 with the gas phase may at best be described by

$$\tfrac{1}{2}O_2 + V_O^{\cdot\cdot} + 2e' \rightleftharpoons O_O. \quad (3)$$

The total enthalpy of this reaction is not known. As is usual in semiconductor physics we split this reaction into a virtual incorporation of neutral oxygen

$$\tfrac{1}{2}O_2 + V_O \rightleftharpoons O_O \quad (4)$$

and into subsequent ionization reactions

$$V_O \rightleftharpoons V_O^{\cdot} + e' \quad (5)$$

and

$$V_O^{\cdot} \rightleftharpoons V_O^{\cdot\cdot} + e'. \quad (6)$$

Enthalpies of reactions (4) and (5) have been determined to be about 30 and 150 meV, respectively (*2, 3*).

For higher temperatures and partial pressures, Fermi–Dirac statistics may be replaced by Boltzmann statistics. As a consequence, the chemical potential of all defects can be written as a logarithmic function of the molar concentration, and the mass action formalism can be applied to describe thermodynamic equilibrium. It is worth noting that each electronic defect introduces a standard value which is weakly temperature dependent because of the continuous density of states. In the simplest case, the standard concentration is proportional to $T^{3/2}$. This standard value is incorporated into the mass action constants.

The following cases can be distinguished, if oxygen defects are assumed to be fully ionized:

Pure material (*case i*). According to the above assumptions, the electroneutrality equation for the bulk demands that $[e'] = 2[V_O^{\cdot\cdot}]$. Hence under thermodynamic equilibrium conditions we obtain

$$[e'] = 2^{1/3}K_O^{-1/3}P^{-1/6} \quad (7)$$

Here, K_O is the mass action constant of Eq. (3), P holds for $P(O_2)$, and the brackets denote molar concentrations.

Acceptor-doped material (*case ii*). For immobile acceptor impurities ($A^{a'}$) (or for frozen-in tin vacancies or oxygen interstitials) the $V_O^{\cdot\cdot}$ concentration is fixed:

$$a[A^{a'}] = 2[V_O^{\cdot\cdot}].$$

Hence it follows that

$$[e'] = \left(\frac{2}{a}\right)^{1/2}[A^{a'}]^{-1/2}K_O^{-1/2}P^{-1/4}. \quad (8)$$

Donor-compensated material (*case iii*). For high donor ($D^{d\cdot}$) densities, the e' concentration is fixed [with only slight variations that result from the influence of the equilibria in Eqs. (5) and (6)]. This leads to

$$[e'] = d[D^{d\cdot}]K_O^0P^0. \quad (9)$$

4.2. Partial Pressure Dependence

Since the mass action constants as well as the mobilities are independent of defect concentrations and of component activities for a sufficient dilution, we find that the pressure dependence of the concentration of electrons and of the electronic conductivity can be described by

$$\left(\frac{\partial \ln[e']}{\partial \ln P}\right)_T = \left(\frac{\partial \ln \sigma}{\partial \ln P}\right)_T = N$$
$$= \begin{cases} -\frac{1}{6} \text{ for case i} \\ -\frac{1}{4} \text{ for case ii} \\ 0 \text{ for case iii.} \end{cases} \quad (10)$$

Our examples with different samples are completely reversible. The corresponding impurity concentrations were independent of temperature and O_2 partial pressure values. Therefore, intrinsic behavior, as described in case i, is favored by increasing T and decreasing P.

4.3. Temperature Dependence of σ Values

The temperature dependence of σ contains two contributions.

(I) The temperature dependence of the concentration of free electrons $[e']$ is determined by the temperature dependence of the mass action constant with

$$-R\left(\frac{\partial \ln[e']}{\partial 1/T}\right)_P = \gamma\Delta H_O^0 + \alpha RT \approx \gamma\Delta H_O^0 \tag{11}$$

where ΔH_O^0 is the enthalpy of the reaction in Eq. (3). The factor γ is $\frac{1}{2}$ for case i, $\frac{1}{3}$ for case ii, and zero for case iii. The term αRT accounts for the contribution from the effective density of states; typically $\alpha \approx \frac{1}{3}$ for case i, $\alpha \approx \frac{3}{4}$ for case ii, $\alpha \approx 0$ for case iii. This term may be neglected to a first approximation.

(II) The temperature dependence of the mobility u_j of a defect j can be represented by

$$u_j = u_{j0}(T)\exp(-g_j/RT) \tag{12}$$

where g_j is the free activation enthalpy for migration, which is zero for a band mechanism and nonzero for a hopping mechanism in polaron or impurity conduction. For band conduction, μ_{j0} accounts for the hindering of electron transport by phonon scattering. In the acoustic mode, $u_{j0} \sim T^{-1.5}$ holds. The scattering mechanism in SnO_2 is a matter of controversy (*3–5, 9, 18, 19*). At lower temperatures in particular, the mechanisms seems to be complicated. Here, u increases with increasing temperature. The high-temperature mechanism seems to be determined by the acoustic mode. The electronic transport properties do, however, differ strongly from sample to sample. This holds particularly for the temperature of maximum mobility (*4*).

In each case, the temperature dependence of σ may formally be described by

$$-R\left(\frac{\partial \ln\sigma}{\partial 1/T}\right)_P = \gamma\Delta H_O^0 + h_{e'} + \alpha' RT \approx \gamma\Delta H_O^0. \tag{13}$$

At high temperatures, $h_{e'} \approx 0$ holds. At lower temperatures, the effective migration enthalpy is still negligible compared with $\gamma\Delta H_O^0$. For $\Delta T^{-1} \approx 10^{-3}$ K^{-1}, the mobility changes by at most one order of magnitude, whereas the concentration of electrons changes by more than ten orders of magnitude (*3–5*). The product $\alpha' RT$ is reduced compared with αRT by the influence of $u_0(T)$. Therefore, the formation term remains the only important one. Only in case iii, with $\gamma = 0$, is the mobility contribution of importance, but in this case deviations from the assumed simple defect chemistry, such as $V_O^{\cdot}$ formation, become important.

4.4. Comparison with Experimental Results

For SnO_2 (Kelpin) we find a linear relation in Fig. 3 between log σ and log P, i.e., a linear relation between ln σ and the oxygen chemical potential. Slopes of $-\frac{1}{4}$ for $T \leq 780$°C and of $-\frac{1}{6}$ for $T \geq 780$°C are observed.

The isotherm at 782°C shows a change in the slope from $-\frac{1}{4}$ at high partial pressures to $-\frac{1}{6}$ at low partial pressures. The behavior can be explained completely within the framework of the above defect model.[1] Thus, the behavior at low temperatures and high partial pressures is controlled by acceptor impurities, or less probably (see Table I) by tin vacancies or oxygen interstitials as described in case i. At high temperatures, the intrinsic defects become important. Consequently we expect the electronic concentration around $T = 780$°C to be of the same order of magnitude as the impurity concentration. In estimating this value with an upper limit of $u = 100$ cm^2 V^{-1} s^{-1} (*4*) and a σ value of 10^{-2} Ω^{-1} cm^{-1} we obtain a defect concentration of at most 10^{-9} mol cm^{-3}. The latter corresponds to a mole fraction of 2×10^{-8} if the molar volume of SnO_2 is assumed to be 21.5 cm^3 mol^{-1}. This fraction is far too low for real impurities (*4*). Since the uncertainties in absolute values of the mobility do not account for this large discrepancy, the above-men-

[1] In spite of some uncertainties in the slopes, it is significant that the absolute intrinsic slope is not greater than $\frac{1}{6}$, so that Sn interstitials ($\geq\frac{1}{5}$) are excluded.

tioned assumption of a strong depression of σ values by porosity effects is supported. Furthermore, foreign impurities are shown to cause an acceptor effect (see Table I) rather than tin vacancies or O interstitials.

An alternative explanation of $-\frac{1}{4}$ slope, assuming the presence of singly ionized oxygen vacancies ($V_O^{\cdot}$) to be predominant, would also be in line with the results discussed so far. It would, however, fail to explain the shape of the critical isotherm in Figs. 3 and 4, as it may be deduced by combining Eqs. (3) and (6) to give

$$O_2 + 2V_O^{\cdot} \rightleftharpoons V_O^{\cdot\cdot} + O_O. \quad (14)$$

A change opposite that from $-\frac{1}{4}$ to $-\frac{1}{6}$ with increasing partial pressure would be expected in this case.

In Fig. 4 the isotherm represented by round symbols represents the results for nominally very pure SnO_2 (Ventron).

The slight changes in the absolute σ values are not significant because of the different porosities and different activation energies of the two samples. Hence, the defect chemistry is regarded as essentially the same. Obviously we have introduced a similar content of impurities during the preparation (see Table I). An equal amount of tin vacancies as compensating defects is less probable because of the different sintering procedures.

Our defect model is supported further by the effect of In doping, as illustrated in Fig. 5. Because of comparable ionic radii (In^{3+}: 80 pm, Sn^{4+}: 70 pm) and because of the electronic configuration of In atoms ($5s^2$ $5p^1$), In occupies in a trivalent state tin sites (*20*) and produces an acceptor effect, hence increasing $V_O^{\cdot\cdot}$ [cf. Eq. (15)] and decreasing [e'] (cf. Fig. 3) as well as σ [cf. Eq. (3)] according to

$$In_2O_3 + 2Sn_{Sn} + O_O \rightleftharpoons 2In_{Sn}' + V_O^{\cdot\cdot} + 2SnO_2. \quad (15)$$

As expected for case ii, the conductivity is depressed by about one order of magnitude and the slopes are $-\frac{1}{4}$ over the entire temperature range (cf. Fig. 5).

The dopant Sb on the other hand, with its ionic radius of 60 pm and its electronic configuration ($5s^2$ $5p^3$), is, because of the high oxygen potential, expected to occupy Sn^{4+} sites as Sb^{5+}. These Sb donor levels are located 35 meV below the conduction band edge (*3*). The donor effect results from

$$Sb_2O_5 + 2Sn_{Sn} + V_O^{\cdot\cdot} \rightleftharpoons 2Sb_{Sn}^{\cdot} + O_O + 2SnO_2. \quad (16)$$

Consequently, the conductivity is enhanced by half an order of magnitude compared with the pure material SnO_2 (Ventron) (see Fig. 3). As is expected from Table I, the Sb content may change the concentration of the minority charge carriers. It is not high enough, however, to alter the influence of the majority charge carriers. Therefore, the pressure dependence corresponds to that of case ii. Consequently, the transition between extrinsic and intrinsic behavior occurs at lower temperatures and at the same conductivity value, i.e., at the same electronic and the same acceptor concentration. The behavior expected for case iii has been realized presumably in the experiments of Ref. (*2*): The slopes observed there are zero below 1000°C and $-\frac{1}{6}$ above 1000°C, with a transition from extrinsic to intrinsic at the critical isotherms from high (O) to low ($-\frac{1}{6}$) partial pressures. In these experiments, the donor effect presumably results from the preparation, i.e., from the chemical vapor deposition of $SnCl_4$ which introduces Cl^-. The latter most probably occupies O^{2-} sites because of comparable ionic radii (180 pm for Cl^- and 140 pm for O^{2-}) according to

$$SnCl_4 + 2V_O^{\cdot\cdot} + 2O_O \rightleftharpoons SnO_2 + 4Cl_O^{\cdot}. \quad (17)$$

For comparison, results from Ref. (*2*) are shown in Fig. 6.

The temperature dependence of measurements at $P = 1$ bar is shown in Fig. 7 for differently doped SnO_2 samples.

At exactly the temperature expected to be the transition temperature for pure oxygen, a kink is observed in the curves of pure and Sb_2O_5-doped (but not In_2O_3-doped) materials. This again is in agreement with the proposed defect model. Moreover, the ratio of the high-temperature slope for SnO_2 (Sb_2O_5) (corresponding to an activation energy of 0.7 eV) to low-temperature slope for SnO_2 (Sb_2O_5) (corresponding to 1.2 eV) is to a good approximation 2:3 as postulated above. The same holds for the slope of pure SnO_2, although in this case just the onset of the high-temperature slope (~1.2 eV) can be seen. Taking the slope for SnO_2 (In_2O_3) (corresponding to 1.9 eV) as an estimation of the extrinsic slope, we estimate the expected ratio 2:3 also for SnO_2 (Kelpin). The scattering in the relevant values is still somewhat puzzling. The large slope of SnO_2 (In_2O_3) cannot be explained by simple association equilibria between In'_{Sn} and $V^{\cdot\cdot}_O$ with their opposite charges. The differences probably result from different porosities or segregation phenomena (see Experimental) rather than from different mobilities. Also, some shrinking of the Pt electrodes was observed during the experiments. Strong deviations at temperatures below 500°C, not discussed here, certainly result from nonequilibrium states (see Section 4.5). The observed slopes in this temperature range correspond to activation energies of 0.3 eV which are in agreement with the literature. They may result from the ionization equilibria of frozen-in oxygen defects and hence from the reaction enthalpies of Eqs. (5) and (6) (*2*).

Samson and Fonstad found activation energies on the order of 1 eV for the intrinsic region which are roughly comparable to ours if the scattering of the data is taken into account. From our analysis we derive a value of ~2.2 eV for ΔH^0_O In Eq. (3). This corresponds to 2 eV for the reaction formulated in Eq. (4) [neglect of αT in Eq. (13) is justified by the fact that nearly the same slopes are obtained in a $\log(\sigma T^{3/2})$—instead of $\log \sigma$—plot]. The energy values known so far are plotted in Fig. 8. The absolute values are related to the formation of one electron.

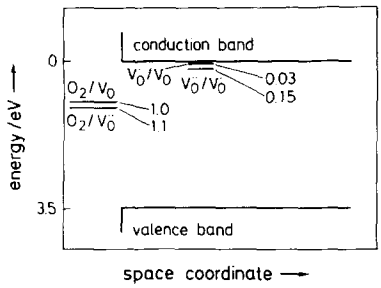

FIG. 8. Energy levels of the system SnO_2/O_2 with respect to SnO bulk. The donor levels and the band gap are taken from Ref. (*2*, *8*). A flat band situation is assumed.

Lack of knowledge of precise absolute values does not allow the calculation of reaction entropies and mass action constants. This will be discussed elsewhere.

4.5. Time Dependence of Oxygen Equilibration

Assuming $V^{\cdot\cdot}_O$ and e' to be the mobile defects in the temperature range of the present study, the equilibration of SnO_2 with oxygen in the gas phase occurs by simultaneous diffusion of $V^{\cdot\cdot}_O$ and $2e'$. Since the electrons move considerably faster, the diffusion coefficient (or the mobility) of oxygen vacancies is the rate-limiting factor. The equilibration times t_{eq} for our samples (pellets 1 mm thick, 1 cm in diameter) were of the order of a minute at 900°C, of an hour at 700°C, and of a day at 600°C. Assuming an average particle diameter of 2 μm, and fast O_2 pore diffusion to each grain because of the high porosity, we take the grain diameter as the characteristic diffusion length L. To a rough estimate the diffusion coefficient D is given by setting the mean square displacement equal to the diffusion length. We estimate diffusion coefficients of oxygen vacancies on the order of 10^{-10} to 10^{-9}

$cm^2\ s^{-1}$ for 900°C, 10^{-12} to 10^{-11} for 700°C, and 10^{-13} for 600°C. For samples of millimeter size, t_{eq} would be expected to be about 100 days at $T = 900$°C which is far longer than observed experimentally on single crystals (*2*). On the other hand, the assumption of sample thickness as the characteristic diffusion length yields diffusion coefficients that are too high. We therefore assume that pore diffusion is not fast with respect to chemical volume diffusion effects in the whole sample at high temperatures. This is supported by the observation that a thicker sample with comparable porosity and grain size shows a slower response to a sudden $P(O_2)$ change but a similar response to a temperature change. A more detailed analysis (*21*) requires the control of grain boundary conditions and will be investigated thoroughly in the future.

Acknowledgments

We thank O. Buresch and L. Viczian for performance of the chemical analysis and the X-ray investigations, and B. Reichert and S. Prill for technical assistance during the experiments.

References

1. W. Göpel, *Prog. Surf. Sci.* **20,** 9 (1986).
2. S. Samson and C. G. Fonstadt, *J. Appl. Phys.* **44,** 4618 (1973).
3. C. G. Fonstadt and R. H. Rediker, *J. Appl. Phys.* **42,** 2911 (1971).
4. H. J. van Daal, *Solid State Commun.* **6,** 5 (1968).
5. E. E. Kohnke, *J. Phys. Chem. Solids* **23,** 1557 (1962).
6. T. Sasaki and H. Hijitikata, *Nippon Daigaku Bunrigakubu Shizenkagaku Kenkyusho Kenkyo Kigo* **10,** 1 (1975).
7. M. Foex, *Bull. Soc. Chem. Fr.* **11,** 6 (1962).
8. "Gmelin's Handbuch der anorganischen Chemie," Zinn Teil C1, Vol. 46, Verlag Chemie, Weinheim (1972).
9. M. Nagasawa and S. Shinoya, *Phys. Rev. C* **21,** 1070 (1968); A. Svane and E. Antoncik, *J. Phys. Chem. Solids* **48,** 171 (1987).
10. H. Koch, *Phys. Status Solidi* **3,** 1059 (1963).
11. L. Nanis and G. A. Advani, *Int. J. Electron.* **52,** 345 (1982).
12. Y. Mizokawa and S. Nakamura, *Japan. J. Appl. Phys.* **14,** 779 (1975).
13. T. Sakurai and T. Takizdwa, *High Temp. High Press.*, **3,** 325 (1971).
14. O. Kubaschewski, E. L. Evans, and C. B. Alcock, "Metallurgical Thermochemistry," Pergamon, London (1967).
15. S. J. Park, K. Hirota, and H. Yamamura, *Ceram. Int.* **10,** 116 (1984).
16. J. Maier, *Ber. Bunsenges. Phys. Chem.* **90,** 26 (1986).
17. J. Maier, *Mater. Res. Bull.* **20,** 383 (1985).
18. D. A. Wright, *Proc. Br. Ceram. Soc.* **10,** 103 (1968).
19. J. A. Marley and R. C. Dockerty, *Phys. Rev. A* **140,** 304 (1965).
20. J. L. Bates, C. W. Griffin, D. D. Marchant, and J. E. Garnier, *Amer. Ceram. Soc. Bull.* **65,** 673 (1986).
21. J. Maier, *Z. Phys. Chem. N.F.* **140,** 191 (1984).